Theoretical assignment of the Clements bands of SO 2

Camille Lévêque, Richard Taïeb, Horst Köppel

Theoretical assignment of the Clements bands of SO_2

Camille Lévêque[1,2,3,*], Richard Taïeb[2,3], and Horst Köppel[1]

[1] *Theoretische Chemie, Physikalisch-Chemisches Institut, Universität Heidelberg, Im Neuenheimer Feld 229, D-69120 Heidelberg, Germany*

[2] *Sorbonne Universités, UPMC Univ. Paris 06, Laboratoire de Chimie Physique-Matière et Rayonnement, UMR 7614, 11 Rue Pierre et Marie Curie, 75231 Paris Cedex 05, France*

[3] *CNRS, Laboratoire de Chimie Physique-Matière et Rayonnement, UMR 7614, 11 Rue Pierre et Marie Curie, 75231 Paris Cedex 05, France*

[*] *Present address: Department of Physics and Astronomy, Aarhus University, 8000 Aarhus C, Denmark*

The photoabsorption spectrum of SO_2 is theoretically investigated in the energy range 3.56-4.05 eV (28713 - 32665 cm^{-1}). The lowest vibronic levels of the coupled excited electronic states ($1^1A_2/1^1B_1$) have been computed using Lanczos diagonalization of the Hamiltonian. The potential energy surfaces and the diabatization scheme used here were already successfully applied to describe the non-adiabatic dynamics of the molecule [C. Lévêque *et al.* J. Chem. Phys. **138**, 044320 (2013)]. The important vibronic states, playing a role in the experimental spectrum, have been analyzed according to their nodal pattern to propose the first theoretical assignment of the low-energy part of the spectrum. The Clements bands A to D have been assigned and exhibit contributions from numerous transitions, in the low resolution spectrum. The overlap of these transitions is shown to provide an "accidental" regularity of the Clements bands with respect to their intensities, while their regular energy spacing (~ 220 cm^{-1}) results from a unique series (4,n_2,1).

Corresponding author: Camille Lévêque

Email: Camille.Leveque@pci.uni-heidelberg.de

Phone: 00 45 87155643

I. INTRODUCTION

The electronic absorption spectrum of the sulfur dioxide molecule represented one of the first attempts of investigating the ultra-violet spectrum of a triatomic molecule in the 1930's. At low resolution, the absorption spectrum, in the energy range of 3.2-4.7 eV, exhibits intense, regular and sharp absorption bands, followed by an irregular plateau-like regime with roughly constant intensities and ending up at high energy with a pseudo-continuum of absorption. In the first analyses performed by Watson and Parker [1], Clements [2], Asundi and Samuel [3] and Metropolis [4], the authors pointed out that this band system results from one excited electronic state, and according to its intensity to a allowed transition. Numerous debates concerning the energy of the vibrationless transition and the assignment of the bands emerged at this time. Depending on the interpretation of the authors, the vibrationless transition could vary by 0.45 eV [3, 4].

These difficulties have been partially resolved by the work of Douglas [5], who observed a Zeeman effect in the presence of a magnetic field in the low energy part of the spectrum, $3.1 - 3.65$ eV. This effect results from a forbidden transition to a triplet excited state, determined later as a $^3B_1$ state by the rotational analysis of Merer [6]. This absorption band, known usually as the "forbidden band", masks the vibrationless transition of the allowed one. The theoretical work of Hillier and Saunders [7] provided the first SCF calculation of the molecule and predicted the presence of three triplet states and two singlet states in this energy range. The isotopic study of Brand and Nanes [8] clearly showed the two band systems belonging to the triplet states and the singlet states. But, because of the intensity of the spectrum, they discarded the possible role of a vibronic coupling between the 1^1B_1 and 1^1A_2 states to explain the absorption features. Their analysis provided a new assignment of the vibrationless transition at 3.50 eV (28 238 cm^{-1}). A few years later, the rotational analysis of Hamada and Merer [9] established a new energy of the latter at 3.46 eV (27 930 cm^{-1}), with the first experimental evidence of the primordial role of the 1^1A_2 state [10].

This long history provides the basis of our understanding of the molecular spectrum, and starting from the 1990's, a large amount of work studying the Potential Energy Surfaces (PES) of the involved states followed [11–13]. At this time the first wave-packet propagation was performed [14] and showed a fast transfer of population from the initial 1^1B_1 to the 1^1A_2 state, owing to the non-adiabatic coupling between them. New simulations [15] allowed only recently to obtain the spectrum with a good accuracy. Owing to its key role in many fields [16–18], the investigation of the photophysics of SO_2 still attracts great experimental and theoretical interest. As an example, recently, the role of the triplet states have been investigated [19–22], and the role of the 1^3B_2 state

has been established theoretically and experimentally [20, 22–24].

In order to provide a comprehensive description of the photoabsorption spectrum, we investigate here the vibronic transitions in the low-energy part (3.56-4.05 eV) of the spectrum. The analysis of the nodal pattern of the eigenstates of the coupled ($1^1A_2/1^1B_1$) states provides us with the first theoretical assignment of the spectrum. This paper is organized as follows. We present in Section II the theoretical methodology used for computing the diabatic PES and for determining the eigenstates of the molecular Hamiltonian. Section III contains a discussion of the results obtained, followed by some concluding remarks in Sec. IV.

II. COMPUTATIONAL DETAILS

A. Adiabatic potential energy surfaces

Here we summarize the main aspects of our methodology, which has been described in our previous work [15]. The photoabsorption spectrum can be described by considering three electronic states, namely the ground state 1^1A_1 and the two first singlet excited states 1^1B_1 and 1^1A_2. These states have been computed using the MultiReference Configuration Interaction (MRCI) method followed by a Davidson correction [25, 26]. For each state the initial wavefunction results from a state-averaged complete active space self-consistent field (CASSCF) calculation, including 18 active electrons in 12 orbitals. The molecular orbitals are described in the correlation-consistent polarized valence triple-zeta (cc-pVTZ) primitive basis set for the sulfur and oxygen atoms [27]. The relative position of the atoms is described using a combination of the internal coordinates, namely $R_s = (R_1 + R_2)/2$ and $Q_u = (R_1 - R_2)/2$, where $R_{1,2}$ stands for the distance between the sulfur and the oxygen atoms, in addition to the $\widehat{OSO}$ angle ϕ, see Fig. 1. The variation of these three coordinates is used to build the three dimensional PES of each electronic states. In addition, the transition dipole moments between the electronic ground state and the two electronic excited states have been computed at the MRCI level as a function of the nuclear coordinates. In C_{2v} symmetry, the only allowed transition is obtained between the GS and the 1^1B_1 state, as expected from symmetry rules, but in C_s symmetry a weak transition dipole moment is obtained for the transition to the 1^1A_2 state. These dipoles are used to study the non-Condon effects in the spectrum.

The two excited electronic states 1^1B_1 and 1^1A_2 are coupled through a *symmetry-allowed* conical intersection [28], which mixes the two adiabatic states for an asymmetric distortion of

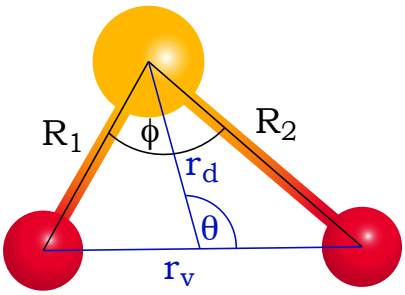

FIG. 1: Definition of the two sets of coordinates used throughout this work. In black, the two SO bond lengths R_1 and R_2 and the $\widehat{OSO}$ angle ϕ represent the internal coordinates which have been used to compute the PES. In blue, r_v , r_d, and θ represent the Jacobi coordinates used to express the kinetic energy operator.

the molecule. Such a distortion lowers the C_{2v} symmetry of the system to the C_s point group, where the two states are of A" symmetry. In the C_{2v} plane ($Q_u = 0$), the two states exhibit a crossing along a *seam* for values $110 < \phi < 120°$ as a function of R_s (see Fig. 2). This situation leads to a non-adiabatic coupling, resulting from the action of the nuclear kinetic energy operator on the electronic wavefunctions depending parametrically on the nuclear coordinates. This coupling exhibits a singularity at the conical intersections breaking down the Born-Oppenheimer approximation. Hence, the two electronic states must be considered together [28–31]. Moreover a numerical treatment and evaluation of the singularity is not a simple task and a transformation of the electronic basis functions to avoid such a singularity is preferable.

B. Diabatic Hamiltonian

The transformation from the adiabatic to a diabatic electronic basis has been performed using the regularized diabatization scheme [32, 33], which consists of an unitary transformation of the electronic basis. The advantage of this method is that the unitary transformation can be defined exclusively from the knowledge of the adiabatic PES only, and has been successfully applied for different systems [34–38]. Collecting the nuclear coordinates in a vector $\mathbf{Q}$, we label the regularized diabatic potential matrix of the two electronic states, $\mathbf{W}_{reg}(\mathbf{Q})$, as follows:

$$\boldsymbol{W}_{reg}(\boldsymbol{Q}) = \Sigma(\boldsymbol{Q})\mathbf{1} + \begin{pmatrix} d(\boldsymbol{Q}) & c(\boldsymbol{Q}) \\ c(\boldsymbol{Q}) & -d(\boldsymbol{Q}) \end{pmatrix}, \tag{1}$$

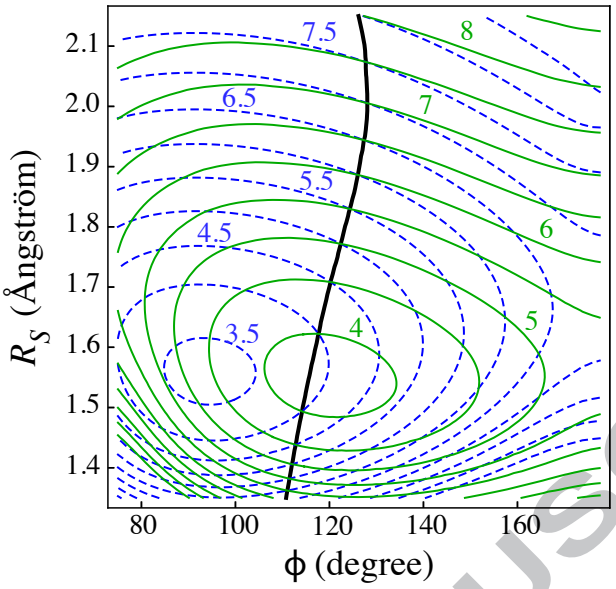

FIG. 2: Potential energy surfaces of the 1^1A_2 (dashed blue) and 1^1B_1 (green) states with respect to R_S and ϕ. The seam of conical intersections is displayed by the black line. The isolines are energetically spaced by 0.5 eV for both states.

namely the sum of a diagonal matrix $\Sigma(\boldsymbol{Q})$ and a traceless one. The unknown elements of the diabatic potential matrix can be obtained by transforming it back to the adiabatic basis, i.e. performing a diagonalization,

$$\boldsymbol{V}(\boldsymbol{Q}) = \boldsymbol{S}(\boldsymbol{Q})^{\dagger}\boldsymbol{W}_{reg}(\boldsymbol{Q})\boldsymbol{S}(\boldsymbol{Q}) \tag{2}$$

by means of a unitary transformation $\mathbf{S}(\mathbf{Q})$. The diagonal part of the diabatic potential is identified with the half sum of the adiabatic PES, $\Sigma(\boldsymbol{Q}) = (V_1(\boldsymbol{Q}) + V_2(\boldsymbol{Q}))/2$. The elements of the traceless matrix are linked to their half difference ($\Delta(\boldsymbol{Q}) = (V_1(\boldsymbol{Q}) - V_2(\boldsymbol{Q}))/2$), through the relation $\Delta(\boldsymbol{Q}) = \sqrt{c^2(\boldsymbol{Q}) + d^2(\boldsymbol{Q})}$. Using a first order (linear) Taylor expansion of the diabatic potential around the locus of the conical intersection ($\boldsymbol{Q_0}$) and the symmetry of the system, the elements $c(\boldsymbol{Q})$ and $d(\boldsymbol{Q})$ can be determined by,

$$\begin{pmatrix} d(\boldsymbol{Q}) & c(\boldsymbol{Q}) \\ c(\boldsymbol{Q}) & -d(\boldsymbol{Q}) \end{pmatrix} = \frac{\Delta(\boldsymbol{Q})}{\sqrt{\Delta_0^2(\boldsymbol{Q_g}) + (\lambda Q_u)^2}} \begin{pmatrix} \Delta_0(\boldsymbol{Q_g}) & \lambda Q_u \\ \lambda Q_u & -\Delta_0(\boldsymbol{Q_g}) \end{pmatrix}, \tag{3}$$

where we have introduced $\boldsymbol{Q_g} = (R_s, \phi)$, which collects the symmetric displacements of the nuclei and $\Delta_0(\boldsymbol{Q_g})$ the half difference of the adiabatic PES in the C_{2v} subspace only. The quantity λ is

evaluated as the derivative of $\Delta(\boldsymbol{Q_g}, Q_u)$ with respect to Q_u at the degeneracy, i.e.

$$\lambda = \left.\frac{\partial \Delta(\boldsymbol{Q})}{\partial Q_u}\right|_{\mathbf{Q}=\mathbf{Q_0}}. \tag{4}$$

A discussion concerning the evaluation of λ can be found in Ref. [15]. Assuming that the nuclear kinetic energy operator is diagonal in this basis, the Hamiltonian of the system reads,

$$\boldsymbol{H}(\boldsymbol{Q}) = T_N(\boldsymbol{Q})\mathbf{1} + \boldsymbol{W}_{reg}(\boldsymbol{Q}). \tag{5}$$

The diabatic PES of the 1^1B_1 and 1^1A_2 states have been subsequently fitted [15], and transformed into a set of symmetry adapted Jacobi coordinates $(\boldsymbol{r}_d, \boldsymbol{r}_v, \theta)$ (see Fig. 1). For a total angular momentum $J = 0$, the nuclear kinetic energy operator, T_N, is expressed as:

$$\hat{T}_N = -\frac{1}{2\mu r_d}\frac{\partial^2}{\partial r_d^2} r_d - \frac{1}{2Mr_v}\frac{\partial^2}{\partial r_v^2} r_v - \frac{1}{2I_\theta \sin\theta}\frac{\partial}{\partial\theta}\sin\theta\frac{\partial}{\partial\theta} \tag{6}$$

where we have introduced,

$$M = \frac{1}{2}m_O;\ \mu = \frac{2m_S m_O}{m_S + 2m_O};\ I_\theta = \left[\frac{1}{Mr_v^2} + \frac{1}{\mu r_d^2}\right]^{-1} \tag{7}$$

with m_O and m_S the masses of the oxygen and of the sulfur atoms, respectively, and I_θ the three-body moment of inertia. It is worth mentioning here that we have used the standard atomic masses for both the sulfur and oxygen atoms, and not the isotopic ones. Further work on the specific isotopologue could benefit to the understanding of the mass-independent fraction of the molecule [16, 39–42].

Finally, the adiabatic transition dipole moments have been transformed to the diabatic representation and interpolated to evaluate them in Jacobi coordinates. The above methodology has been already successfully used to describe the nuclear wavepacket dynamics on the coupled $1^1B_1/1^1A_2$ states [15].

C. Lanczos diagonalization

Here we propose the inspection of the eigenstates of the molecular Hamiltonian, which leads to new physical insight onto the dynamics. The Hamiltonian has been discretized using a discrete-variable representation (DVR), consisting of 130 Hermite quadrature points for $\boldsymbol{r}_v$ extending from

3.4 to 6.3 Bohr and 80 for the $\boldsymbol{r}_d$ coordinate from 0.63 to 2.8 Bohr. The θ angle as been described using 73 Legendre polynomials, spanning $0.99 < \theta < 2.15$ radian. The number and the range of the DVR is the same as that used for the wavepacket dynamics in Ref. [15].

The diagonalization of the Hamiltonian has been performed using the Lanczos recursion algorithm [43] as implemented in the Heidelberg MCTDH package [44–47]. The method relies on the construction and simultaneous orthonormalization of an approximate Krylov space obtained from the successive application of the Hamiltonian on an initial vector. Introducing $|u_0\rangle$ as the initial vector of the Lanczos recursion scheme, the subsequent Lanczos vectors are determined using [47],

$$\beta_{n+1}|u_{n+1}\rangle = (\hat{\mathbf{H}} - \alpha_n)|u_n\rangle - \beta_n|u_{n-1}\rangle, \tag{8}$$

i.e., a three-term recurrence relation with:

$$\alpha_n = \langle u_n|\hat{\mathbf{H}}|u_n\rangle \ ; \ \beta_0 = 0 \text{ and } \langle u_n|u_m\rangle = \delta_{nm}. \tag{9}$$

This scheme transforms iteratively the Hamiltonian into a tridiagonal matrix in the Lanczos basis, named hereafter the Lanczos matrix ($\mathbf{L}$), and allows an efficient diagonalization with a low storage requirement.

The eigenvalues of the Hamiltonian can be obtained directly from the diagonalization of the Lanczos matrix,

$$\mathbf{U}^{-1}\mathbf{L}\mathbf{U} = \mathbf{E} \tag{10}$$

where $\mathbf{E}$ is the diagonal matrix of the common eigenvalues of the Hamiltonian and the Lanczos matrix, and $\mathbf{U}$ is the matrix of the eigenvectors of $\mathbf{L}$. The eigenstates of the Hamiltonian can then be obtained as a linear combination of the Lanczos vectors weighted by the eigenvectors of the Lanczos matrix [48], i.e.,

$$|\Psi_{E_{nn}}\rangle = \sum_{m}^{M} \mathbf{U}_{nm}|u_m\rangle \tag{11}$$

with $|\Psi_{E_{nn}}\rangle$ the eigenstate corresponding to the eigenvalue E_{nn}.

While storing the Lanczos vectors is not possible, except for a small Krylov subspace, the storage of the eigenvectors of the Lanczos matrix is feasible. Thus a first computation is performed to obtain the eigenvalues and eigenvectors of the Lanczos matrix, and a subsequent Lanczos reduction

is performed to construct a selected set of eigenstates of the Hamiltonian in the DVR basis. To ensure the convergence of the results, we have used a variable number of iterations M, i.e. different sizes of the Krylov subspace. The results presented have been obtained for 45000 iterations and only eigenstates and eigenvalues identical to the ones obtained for 40000 iterations are discussed. We are interested in the photoabsorption spectrum of the molecule rather than the eigenstates of the Hamiltonian. Thus we used $|u_0\rangle = |\Psi_{GS}\rangle$, i.e. the vibrational GS of the system, because it provides an efficient computation of the intensities of the photoabsorption spectrum without storing the Lanczos vectors [49].

D. Spectral quantization

In addition to the Lanczos diagonalization method, a spectral quantization treatment has been used to investigate the quasi-resonant states of the photoabsorption spectrum. This method has first been introduced by M. Feit *et al.* [50] for bound state systems and successfully applied to scattering problems [51–54]. The aim of the method is to provide an alternative way to study the eigenstates of the Hamiltonian using a time-dependent formalism. The time-dependent wavefunction $|\chi(t)\rangle$, obtained from the numerical propagation of an initial wavepacket $|\chi(0)\rangle$, is first used to evaluate the autocorrelation function $C(t) = \langle\chi(0)|\chi(t)\rangle$ and subsequently the spectral intensity $I(E)$ from its Fourier transform. Using as an initial condition $|\chi(0)\rangle = |\Psi_{GS}\rangle$, we obtain nothing else than the photoabsorption spectrum of the system. From this spectrum, the energies of the resonant states appear as peaks in $I(E)$ and are used to extract the resonant energies E_n^{qr} of the quasi-resonant states of interest. The states themselves are obtained by evaluating,

$$\langle \mathbf{x}|\Psi^{qr}_{E_n^{qr}}\rangle = \int_0^T \langle \mathbf{x}|\chi(t)\rangle w(t) e^{iE_n^{qr}t} dt, \tag{12}$$

for each eigenvalue E_n, where we introduced the final time of the propagation T and a window function $w(t)$ defined by

$$w(t) = \cos^k\left(\frac{\pi t}{2T}\right)\theta\left(1 - \frac{|t|}{T}\right) \tag{13}$$

with $k = 0, 1, 2$ or 3 and $\theta(x)$ the Heaviside function. The notion of quasi-resonant states and energies has been used and is specified by the superscript "qr", because the method involves the conjugate variables E_n and t to determine $|\Psi^{qr}_{E_n^{qr}}\rangle$ and E_n^{qr}. Thus the resonant energies E_n^{qr} converge

to the eigenvalues E_n in the limit of $T \to +\infty$ and the quasi-resonant states converge to the eigenstates of $\hat{\mathbf{H}}$ in the same limit.

In order to obtain a correct resolution of the quasi-resonant states, the time-dependent wavefunction, $|\chi(t)\rangle$, has been propagated until 1 picosecond by solving the time-dependent Schrödinger equation numerically using the diabatic Hamiltonian introduced in Sec. II B and the DVR of Sec. II C (see Ref. [15] for more details). We mainly used this method to ensure the correctness of the eigenstates obtained using the Lanczos diagonalization, but it also provides additional information on the Clements bands E and F.

III. RESULTS AND DISCUSSION

The eigenstates of the Hamiltonian are expanded as a linear combinations of vibrational wavefunctions for the two different diabatic electronic states 1^1A_2 and 1^1B_1. The transition from the electronic ground state is only allowed to the 1^1B_1 excited state, according to the selection rules. The transition probabilities are thus proportional to the Franck-Condon (FC) factors considering the vibrationless ground state (0',0',0') and the vibrational component of the 1^1B_1 electronic state. Hereafter, the transition probabilities will be referred to as intensities and are displayed in Table I. In the energy range considered ~ 200 eigenfunctions have been obtained, but we are interested in the assignment of the experimental spectrum, and not all of them do play a role. Here we report and discuss only the transitions with an intensity larger than 10^{-8}. This limit, between dark and bright states, appears naturally in the low energy part of the spectrum with orders of magnitude difference between their intensities. For energies higher than 3.82 eV, this intensity gap can decrease to two orders of magnitude. Then this limit might seem arbitrary, but the spectrum is still governed by high-intensity lines ($> 10^{-5}$).

In addition to the intensities, we report the relative weights of the different diabatic electronic states in the total wavefunction. It is remarkable that for the energy range considered more than 70% of the wavefunction lies on the 1^1A_2 state, i.e. the forbidden state. And interestingly, for increasing energy, the weight on the 1^1B_1 state increases, but not monotonically. We took advantage of dominant role of the 1^1A_2 diabatic state to assign the spectrum with respect to its vibrational wavefunction only. Each eigenstate of the full Hamiltonian is characterized by a set of quantum numbers (n_1, n_2, n_3), determined from the 1^1A_2 component of the total wavefunction, and reported in Tab. I. The quantum numbers refer to the symmetric stretching, the

TABLE I: Assignment of the low-energy part of the photoabsorption spectrum (3.56 − 4.05 eV) according to the vibrational component wavefunction of the 1^1A_2 state, with n_1, n_2 and n_3 referring to the symmetric stretching, the bending and the asymmetric stretching modes, respectively. In addition, the intensities (FC factors) and the populations in each electronic state are reported. The question marks (?) indicate a tentative assignment.

Energy (eV)	Intensity	$^1A_2/^1B_1$	(n_1,n_2,n_3)	Energy (eV)	Intensity	$^1A_2/^1B_1$	(n_1,n_2,n_3)
3.5631	$2.52\ 10^{-7}$	0.88/0.12	(0,0,1)	3.9274	$2.86\ 10^{-6}$	0.73/0.27	(0,10,1)
3.5967	$2.04\ 10^{-6}$	0.84/0.16	(0,1,1)	3.9280	$1.64\ 10^{-4}$	0.76/0.24	(2,1,3)
3.6309	$5.88\ 10^{-6}$	0.82/0.18	(0,2,1)	3.9298	$3.10\ 10^{-3}$	0.75/0.25	(4,0,1)
3.6551	$5.72\ 10^{-6}$	0.84/0.16	(1,0,1)	3.9367	$2.36\ 10^{-4}$	0.73/0.27	(1,4,3)
3.6661	$7.75\ 10^{-6}$	0.80/0.20	(0,3,1)	3.9383	$2.07\ 10^{-3}$	0.71/0.29	(3,3,1)
3.6889	$2.87\ 10^{-5}$	0.82/0.18	(1,1,1)	3.9416	$5.94\ 10^{-5}$	0.71/0.29	(1,8,1)
3.7017	$1.32\ 10^{-5}$	0.84/0.16	(0,0,3)	3.9467	$2.24\ 10^{-4}$	0.82/0.18	(1,0,5)
3.7024	$1.05\ 10^{-7}$	0.81/0.19	(0,4,1)	3.9541	$2.54\ 10^{-4}$	0.74/0.26	(0,3,5)
3.7238	$6.94\ 10^{-5}$	0.80/0.20	(1,2,1)	3.9545	$3.61\ 10^{-6}$	0.71/0.29	(2,6,1)
3.7367	$2.47\ 10^{-5}$	0.83/0.17	(0,1,3)	3.9560	$9.36\ 10^{-5}$	0.72/0.28	(0,7,3)
3.7389	$1.76\ 10^{-8}$	0.78/0.22	(0,5,1)	3.9600	$3.64\ 10^{-3}$	0.69/0.31	(4,1,1)
3.7488	$5.95\ 10^{-5}$	0.81/0.19	(2,0,1)	3.9615	$3.52\ 10^{-3}$	0.75/0.25	(2,2,3)
3.7592	$8.07\ 10^{-5}$	0.78/0.22	(1,3,1)	3.9658	$1.52\ 10^{-7}$	0.72/0.28	(0,11,1)
3.7721	$3.23\ 10^{-5}$	0.80/0.20	(0,2,3)	3.9707	$5.17\ 10^{-4}$	0.68/0.32	(3,4,1)
3.7759	$2.53\ 10^{-7}$	0.76/0.24	(0,6,1)	3.9729	$2.78\ 10^{-4}$	0.73/0.27	(1,5,3)
3.7825	$2.69\ 10^{-4}$	0.78/0.22	(2,1,1)	3.9785	$1.11\ 10^{-4}$	0.70/0.30	(1,9,1)
3.7951	$5.18\ 10^{-5}$	0.77/0.23	(1,4,1)	3.9797	$6.63\ 10^{-4}$	0.79/0.21	(1,1,5)
3.8004	$2.52\ 10^{-7}$	0.83/0.17	(1,0,3)	3.9884	$6.58\ 10^{-3}$	0.69/0.31	(4,2,1)
3.8079	$2.46\ 10^{-5}$	0.79/0.21	(0,3,3)	3.9893	$1.07\ 10^{-3}$	0.67/0.33	(2,7,1)
3.8133	$4.76\ 10^{-8}$	0.75/0.25	(0,7,1)	3.9907	$6.87\ 10^{-5}$	0.75/0.25	(0,4,5)
3.8164	$5.73\ 10^{-4}$	0.76/0.24	(2,2,1)	3.9914	$1.22\ 10^{-3}$	0.72/0.28	(3,0,3)
3.8312	$5.34\ 10^{-5}$	0.76/0.24	(1,5,1)	3.9938	$5.23\ 10^{-4}$	0.78/0.22	(0,0,7)
3.8323	$9.11\ 10^{-5}$	0.81/0.19	(1,1,3)	3.9959	$8.60\ 10^{-4}$	0.75/0.25	(2,3,3)
3.8397	$3.01\ 10^{-4}$	0.78/0.22	(3,0,1)	4.0043	$7.79\ 10^{-6}$	0.68/0.32	(3,5,1)
3.8443	$5.17\ 10^{-6}$	0.77/0.23	(0,4,3)	4.0044	$5.45\ 10^{-6}$	0.70/0.30	?
3.8457	$2.00\ 10^{-4}$	0.83/0.17	(0,0,5)	4.0083	$1.90\ 10^{-4}$	0.70/0.30	(1,6,3)
3.8508	$3.86\ 10^{-4}$	0.74/0.26	(2,3,1)	4.0138	$2.22\ 10^{-3}$	0.75/0.25	(1,2,5)
3.8512	$2.06\ 10^{-4}$	0.74/0.26	(0,8,1)	4.0156	$1.28\ 10^{-6}$	0.68/0.32	(1,10,1)
3.8664	$1.56\ 10^{-4}$	0.79/0.21	(1,2,3)	4.0161	$5.90\ 10^{-3}$	0.68/0.32	(5,0,1)
3.8680	$5.80\ 10^{-6}$	0.74/ 0.26	(1,6,1)	4.0189	$6.03\ 10^{-3}$	0.71/0.26	(4,3,1)
3.8727	$1.47\ 10^{-3}$	0.75/0.25	(3,1,1)	4.0235	$2.54\ 10^{-6}$	0.70/0.30	(3,1,3)
3.8810	$1.43\ 10^{-7}$	0.76/0.24	(0,5,3)	4.0236	$5.66\ 10^{-6}$	0.64/0.36	(2,8,1)
3.8818	$2.93\ 10^{-4}$	0.81/0.19	(0,1,5)	4.0273	$1.61\ 10^{-7}$	0.73/0.27	(0,5,5)
3.8856	$3.50\ 10^{-4}$	0.72/0.28	(2,4,1)	4.0284	$6.22\ 10^{-4}$	0.71/0.29	(2,4,3)
3.8891	$2.43\ 10^{-6}$	0.73/0.27	(0,9,1)	4.0309	$9.20\ 10^{-5}$	0.73/0.27	(0,9,3)
3.8973	$6.33\ 10^{-4}$	0.80/0.20	(2,0,3)	4.0316	$5.45\ 10^{-8}$	0.77/0.23	(0,1,7)?
3.9016	$1.25\ 10^{-5}$	0.77/0.23	(1,3,3)	4.0384	$1.04\ 10^{-4}$	0.67/0.33	(3,6,1)
3.9046	$1.90\ 10^{-4}$	0.72/0.28	(1,7,1)	4.0429	$2.10\ 10^{-3}$	0.69/0.31	(1,11,1)?
3.9054	$2.59\ 10^{-3}$	0.72/0.28	(3,2,1)	4.0431	$1.04\ 10^{-2}$	0.70/0.30	(4,4,1)
3.9179	$1.74\ 10^{-4}$	0.77/0.23	(0,2,5)	4.0438	$7.64\ 10^{-4}$	0.69/0.31	(1,7,3)
3.9180	$6.84\ 10^{-5}$	0.75/0.25	(0,6,3)	4.0457	$8.26\ 10^{-4}$	0.74/0.26	(1,3,5)
3.9205	$1.50\ 10^{-4}$	0.70/0.30	(2,5,1)				

bending and the asymmetric stretching modes, respectively. To determine these assignments, each bright eigenstate has been plotted as a three-dimensional iso-surface with respect to the Jacobi coordinates, keeping in this way their phase. An illustration is provided in Fig. 3, where we display the different vibrational lobes of the states. Note that, for higher energies, these assignments are only approximate (see also below).

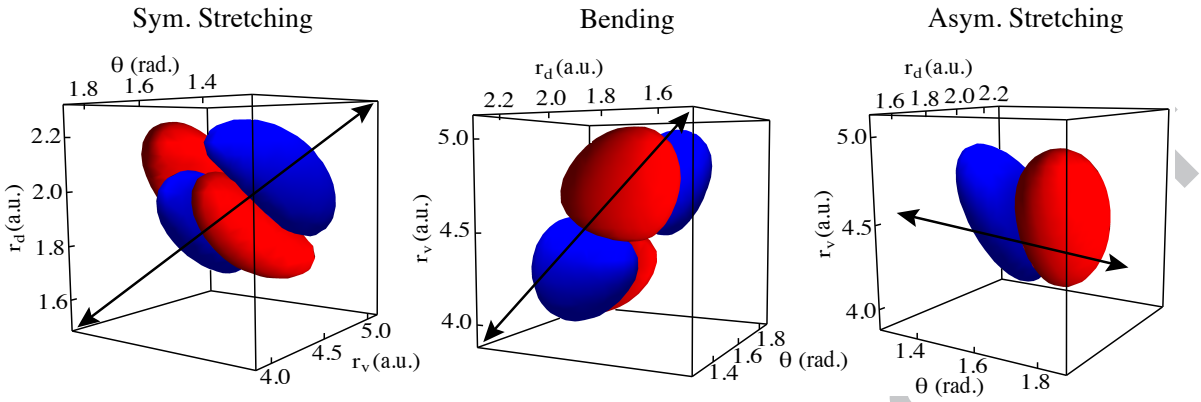

FIG. 3: Representation of isosurfaces ($\Psi_{A2} = \pm 0.002$) of selected vibrational wavefunctions of the coupled electronic 1^1A_2 state in Jacobi coordinates. The sign of the wavefunction is indicated by the color code, positive (negative) values are in red (blue). From left to right are presented the (1,0,1), (0,1,1) and (0,0,1) states.

The first band of the coupled $1^1A_2/1^1B_1$ system is usually assigned at 3.50 eV, according to the extrapolation of Ref. [8] or 3.46 eV according to the rotational study of Ref. [9]. This last value lies in the same energy range as the absorption of the triplet states, and its assignment is not straightforward. We used a global shift (+1945 cm^{-1} including the zero-point-energy correction) of the spectrum to match the envelope of the experimental spectrum and particularly of the Clements bands. In this way, we find the first absorption band, assigned to (0,0,1), at 3.56 eV, which lies higher than the experimental values (see Fig. 3 and Tab. I). It is thus possible that the good overall agreement of our spectrum is accidental and should be shifted back to the red, but this shift does not change our assignment. The vibronic coupling between the two electronic states occurs through the asymmetric stretching mode only. Thus, the vibrational component of the 1^1A_2 electronic state, involved in the absorption spectrum, must contain an odd number of quanta in this mode. Moreover, the FC overlap between the (0',0',0') and the vibrational component of the 1^1B_1 state is not vanishing only for even quanta of asymmetric stretch. Thus, the observed transitions occur to eigenstates with even and odd values of n_3 for the 1^1B_1 and 1^1A_2 components, respectively.

The spectrum exhibits a high density of bright states ($\sim$ 80 in a range of 1 eV), resulting from the large change in the geometry of the molecule between the 1^1A_2 state (R_s = 1.554 Å, ϕ = 94°) and the GS (R_s = 1.448 Å, ϕ = 119.1°), with a difference in the bond angle of 25°. Large quantum numbers have been obtained for the different vibrational modes, with $0 \leq n_1 \leq 5$ for the symmetric stretching, $0 \leq n_2 \leq 11$ for the bending and $1 \leq n_3 \leq 7$ and only odd numbers for the

asymmetric stretching. This mode is highly excited because it leads to the vibronic coupling. In order to compare our results with the experimental ones, we extracted an averaged frequency for the different modes from the first few eigenstates. We obtained $\omega_1 = 730$ cm $^{-1}$ for the symmetric stretching, $\omega_2 = 295$ cm^{-1} for the bending and $\omega_3 = 577$ cm^{-1} for the asymmetric stretching mode. The first two values are in very good agreement with the respective experimental results determined by Brand and Nanes [8].

The different series determined can be analyzed with respect to the relative weight between the 1^1A_2 and 1^1B_1 states and their intensity; they are studied by fixing two of the three quantum numbers and varying the third one. We noticed that the relative weight between the 1^1A_2 and 1^1B_1 states increases monotonically in favor to the 1^1B_1 state, with only few (~ 5) exceptions. As the dipole-allowed transition takes place to the 1^1B_1 state, such an increasing weight can increase the FC factor and thus the intensity of the transition. Indeed, looking at the first members of a series, the intensity increases monotonically as a function of the population in the 1^1B_1 state. But after a certain member of the series, the intensity starts to oscillate despite the fact that the population on the 1^1B_1 state continues to increase. This behavior results from a subtle interplay between the 1^1B_1 population and the nodal structure of the 1^1B_1 vibrational wavefunction, as shown in Fig.4. It is interesting to notice that the wavefunction on the 1^1B_1 electronic state exhibits almost vanishing values in the C_{2v} subspace ($\theta = \pi/2$) but not a node, as explicitly seen in the phase, which does not change its sign. This, at first glance unexpected, feature relates to the double minimum shape of the lowest adiabatic $1^1A_2/1^1B_1$ potential energy surface (see black contour lines of Fig. 6). Given a well depth of 0.0125 eV of each of the two identical C_s symmetric minima, the lowest vibrational levels are localized in either of the wells, and the total wavefunction thus has a minimum at the C_{2v} symmetric barrier, regardless of whether it is a symmetric or antisymmetric linear combination of the two localized vibrational levels.

The energy range studied here spans the first Clements bands, from A to D as indicated in Fig. 5. The first one, band A, lies already ~ 0.4 eV above the first transition and for such energies a large number of different series are observed (see Tab. I and Fig. 5). This complexity of the Clements bands has already been pointed out in the experimental assignments of Hamada *et al.* [9] and Brand *et al.* [8] . The study of the transitions involved in each of the Clements bands shows two important features. First, their regular spacing (~ 220 cm^{-1}) results from the predominant role of the series (4,n$_2$,1) with $1 \leq n_2 \leq 4$, which is consistent with the bending mode energy and the anharmonicity of the PES. Second, the regular increase of the intensity of these bands is

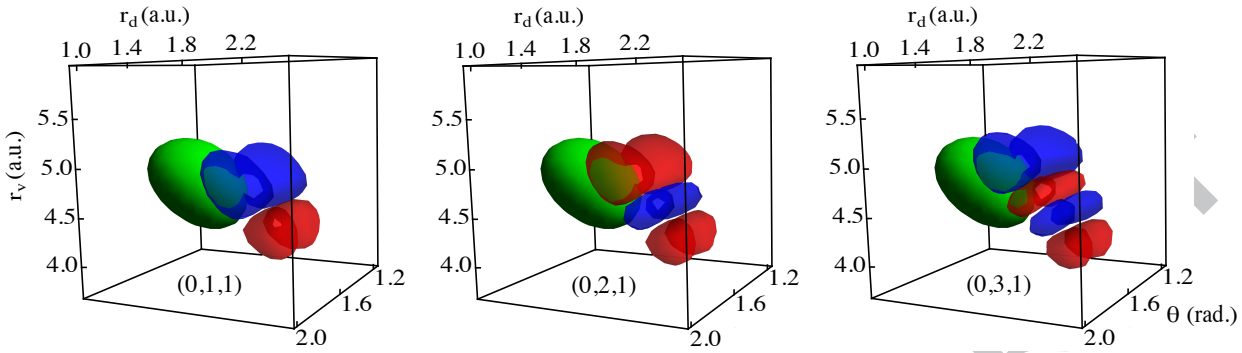

FIG. 4: Representation of the ground state wavefunction (green with $\Psi_{A1} = 0.0001$) and the 1^1B_1 vibrational wavefunction (red and blue with $\Psi_{B1} = \pm 0.0006$) for the series (0,n_2,1) with $n_2 = 1$ to 3. Note that the assignment is based on the vibrational component of the 1^1A_2 electronic state. For increasing values of n_2 lobes of different signs of the 1^1B_1 wavefunction overlap with the GS one.

accidental in the low-resolution spectrum and results from the superposition of different transitions.

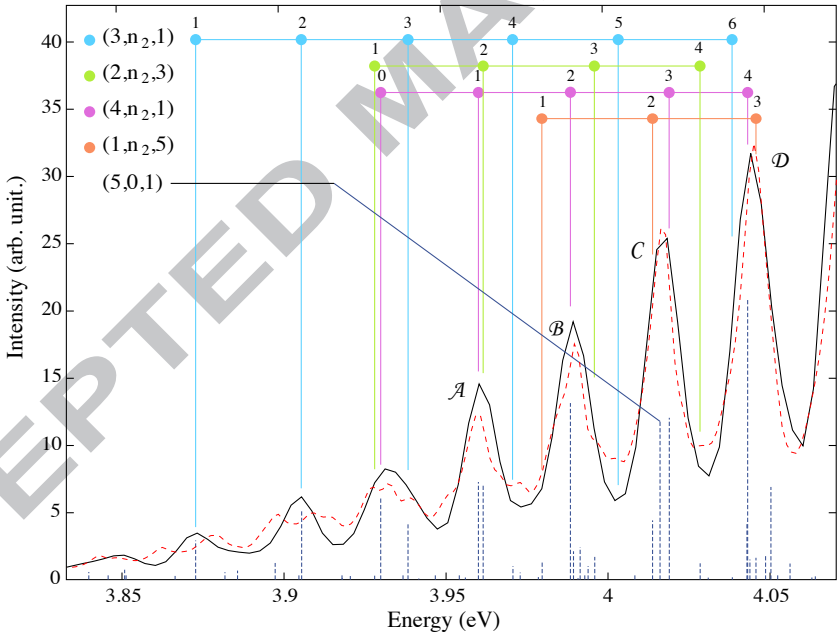

FIG. 5: Summary of the main contributions to the Clements bands A-D. The stick spectrum in dashed lines displays the FC factors reported in Tab. I. Superimposed, the black envelope results from the Fourier transform of the autocorrelation function obtained in Ref. [15], together with the experimental spectrum (dashed red) of Bogumil *et al.*, Ref. [55]. The Clements bands have been labelled according to Ref. [2]. The results from the time-dependent and independent calculations agree with each other very well, which is also true when a larger damping time, i.e. a better energy resolution is used for the calculation of the spectrum from the autocorrelation function. In addition, the agreement with the experiment is particularly satisfying for the Clements bands A-D. Interestingly the Clements bands A and C arise from two almost equally strong excitations, but the bands B and D exhibit one dominant transition.

The analysis of the band A reveals the role of two principal transitions involving the (2,2,3)

and (4,1,1) states with similar intensities (ratio 0.968:1). Band B shows only one predominant transition to the (4,2,1) state and numerous weaker ones involving other final states. The ratio to the next, less intense absorption, i.e. (3,0,3), is 0.186:1. The C band is composed of two transitions of similar intensities to the (5,0,1) and (4,3,1) states (0.978:1), as well as a less intense transition to the (1,2,5) state with a ratio 0.361:1. Finally, the D band is characterized by an intense transition to (4,4,1) with a contribution from the (1,11,1) state at almost identical energy. These results show an important difference in the role of the series (4,n_2,1) in the Clements band B and D, for which it is the dominant transition, and the bands A and C, which exhibit transitions to other states with similar intensities.

The quasi-resonant states of the bands A to D, Fig. 6, have been compared to states obtained from the diagonalization. The quasi-resonant energy for each band has been chosen as the maximum energy of the absorption spectrum obtained from the 1 ps propagation. The propagation time is not long enough to resolve, in the spectrum, the underlying structure of the bands A-C, but it is long enough to partially resolve the band D providing one maximum at 4.043 eV and a second one at 4.05 eV, Fig. 5. Due to the resolution of the spectrum, we cannot expect to obtain from the spectral quantization method the eigenstates but rather a mixture of them. The quasi-resonant states of the bands B and D, which both exhibit one preponderant transition, are actually in very good agreement with the eigenstates (4,2,1) and (4,4,1), respectively. Nonetheless, the transition (4,4,1) lies only ~ 0.002 eV above the (1,11,1) one, and taking a linear combination of these two transitions, weighted with the overlap with the GS (i.e. the square root of the intensity indicated in Tab. I), provides almost a perfect agreement. A similar results are also obtained for the (4,2,1) and (2,7,1) transitions, even if its energy difference between them is slightly larger. The good agreement observed between the quasi-resonant states of the bands B and D and the (4,2,1) and (4,4,1) transition only results from the large ratio of intensity between the different transitions involved in these two bands. The case of the band A and C is more complicated with energetically close transitions with similar intensities. In the case of the band A, the quasi-resonant energy lies at half of the energy difference between the (4,1,1) and (2,2,3) states. The direct comparison of the associated quasi-resonant state and the (4,1,1) eigenfunction exhibits a similar distribution of the density, but with some disagreement. Nonetheless, using, as previously, a linear combination of the two main transitions the quasi-resonant state is recovered. The band C is the more complicated band studied in this work, with three transitions with the same order of magnitude. The quasi-resonant energy is 0.0018 eV below the (4,3,1) transition, closer to the (5,0,1) transition.

In this case, the coefficients of the linear combination of the three eigenstates is not trivial as previously and had required the projection of quasi-resonant state on the eigenfunctions, providing again a good agreement between the time-dependent and independent results.

The previous comparison between the time-dependent and independent results give us the possibility to explore the possible role of the series (4,n_2,1) in the Clements bands E and F using the quasi-resonant states. The assignment of the eigenstates for these energies has not been carried out, but the intensities and energies of the eigenstates of these two bands have been obtained. The band E exhibits a intense transition at 4.0712 eV and a weaker one 0.0019 eV above with a ratio 1:0.12. The band F is more complex with a succession of three partially resolved lines in the spectrum, where each of them is composed of two transitions according to the diagonalization results. The first two transitions include the most intense one at 4.0990 eV, lying 0.0012 eV above the other one with a ratio 0.27:1. The remaining four transitions are obtained at 4.1035, 4.1047, 4.1076 and 4.1094 eV with ratios of 0.28, 0.16, 0.1 and 0.14, respectively, in comparison to the most intense transition. A 2-dimensional representation of these states is displayed in Fig. 6, for a fixed value of ϕ. The node at $Q_u = \pi/2$ is observed also for the bands E and F. In addition, two to five nodes along the R_s coordinate are obtained, depending on the choice of the angle ϕ. This complicated nodal structure partly relates to the contribution of several eigenstates to most Clements band. Upon closer inspection we can see that for band C the nodal lines are indeed nearly parallel to the coordinate axes as one would expect for the set $(4, n_2, 1)$ of quantum numbers. For the others, the main probability density is arranged more along the axis bisectors or in a bent fashion. According to the contour lines of the lower adiabatic PES, also included in the figure, the density follows its double minimum shape, as was already found for the time-dependent wavepacket [14, 15]. We add that a similar behaviour is also obtained for some of the underlying eigenstates, such as the state (4,1,1) contributing to the Clements band A in Fig. 5. In the same cut (i.e. for fixed angle phi) it exhibits a similar nodal pattern as the quasi-resonant state for Clements band B in Fig. 6. When projecting on the R_s and Q_u coordinate axes, the presence of 4 and 1 nodal lines (mentioned in Tab. I and Fig. 5) is clearly visible. Nevertheless the main probability density occurs more along the bent line already mentioned above, where 9 nodal lines are visible (the presence of one node for the bending mode in unambiguous). For the other eigenstates the nodal pattern can be considerably more complicated, especially for energies above 3.9 eV. This presents a limitation to the assignments which can be rather severe for higher energies. More details are currently under investigation and will be published separately.

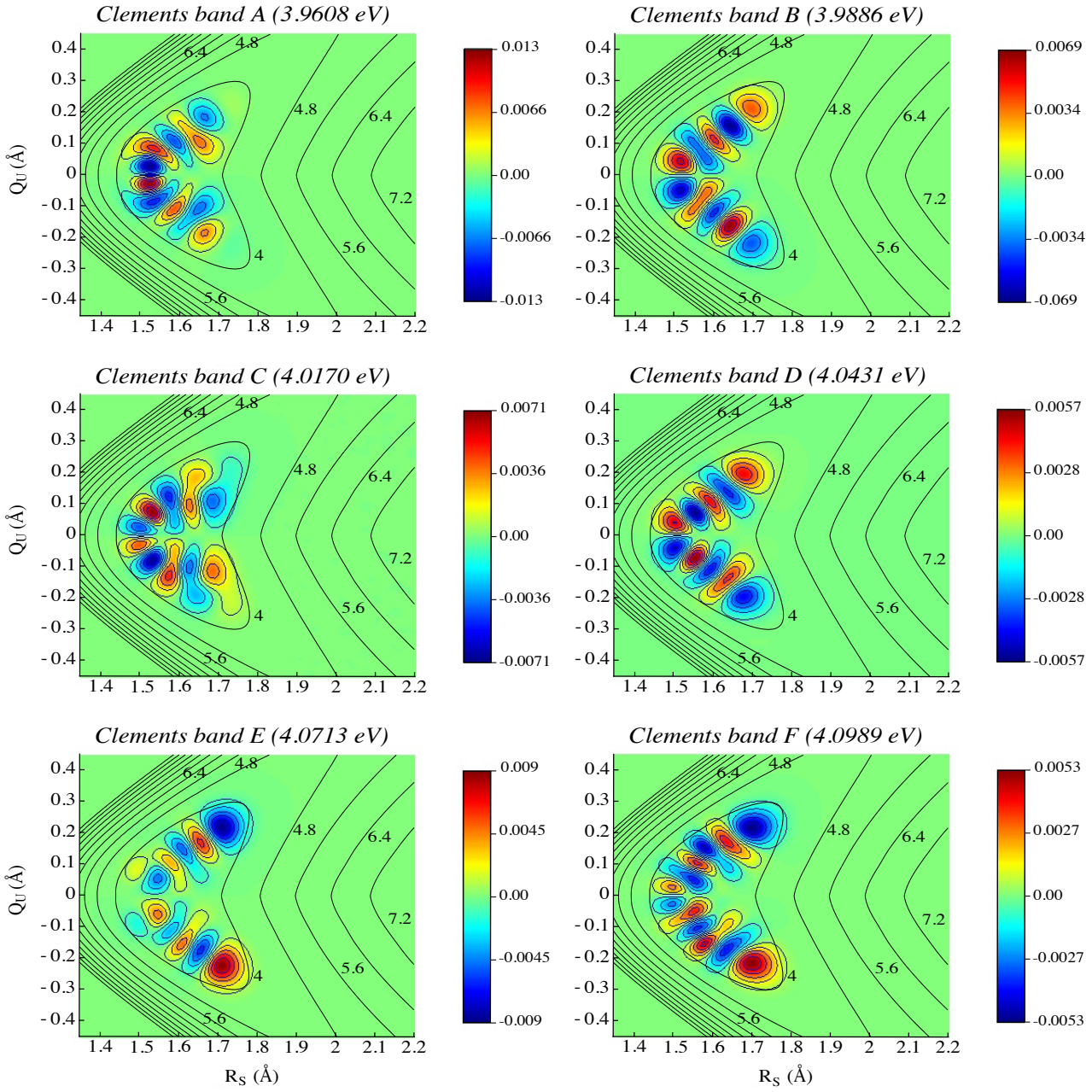

FIG. 6: 2-dimensional representation of the quasi-resonant states for the Clements bands A to F. The wavefunction are displayed as a function of the internal coordinates R_s and Q_u, see Fig. 1, the cold and warm colors indicate the sign of the wavefunction. The lowest adiabatic PES is superimposed in full-black lines, energetically spaced by 0.4 eV. The different values of k in Eq. (13) give similar results and we displayed the one obtained for $k = 0$.

Non-Condon effects may result from the coordinate-dependence of the electronic transition-dipole moment between the GS and the excited states. The GS vibrational wavefunction lies primarily in the C_{2v} subspace, for which the transition dipole to the 1^1A_2 state is vanishing. Thus, we first consider only the transition dipole moment between the GS and the 1^1B_1 state ($\mu_{B_1/GS}$). The new intensities $I_{\mu_{B_1/GS}}(E)$ are computed as

$$I_{\mu_{B_1/GS}}(E) = \left|\langle \Psi_{B_1}(E)|\mu_{B_1/GS}|\Psi_{GS}\rangle\right|^2 . \tag{14}$$

In the energy range considered, the inclusion of the transition dipole moment does not affect the dark states, i.e. no new intense absorption lines appear. In addition, the results are roughly the same as previously with a constant scaling factor ($\sim 2.5\ 10^{-2}$, atomic units are used throughout). In Fig. 7 (a), we display the ratio between the intensities obtained from Eq. (14), with $\mu_{B_1/GS}$ and the FC factors discussed above. Large variation of intensity is observed only for few transitions, assigned in Fig. 7, and occurs only for states with originally very low FC factors. Therefore no change of the global shape of the spectrum is observed.

The role of the transition dipole moment between the GS and the 1^1A_2 state has also been considered because of the important part of the population lying on this electronic state. In this case the spectral intensity $I_{\mu_{B_1A_2/GS}}(E)$ is obtained as,

$$I_{\mu_{B_1A_2/GS}}(E) = \left|\langle \Psi_{B_1}(E)|\mu_{B_1/GS}|\Psi_{GS}\rangle + \langle \Psi_{A_2}(E)|\mu_{A_2/GS}|\Psi_{GS}\rangle\right|^2 . \tag{15}$$

In the same way as previously, the ratio of the intensities and the FC factors is displayed in Fig. 7 (b). This ratio clearly shows that the same transitions as before are affected, with an enhancement of the variation of the intensity. The transition dipole moment affects strongly the transition to states with a high quantum number in the bending and asymmetric stretching modes, but globally the results are similar to the FC factors, which shows that non-Condon effects are not important in the low-energy part of the spectrum.

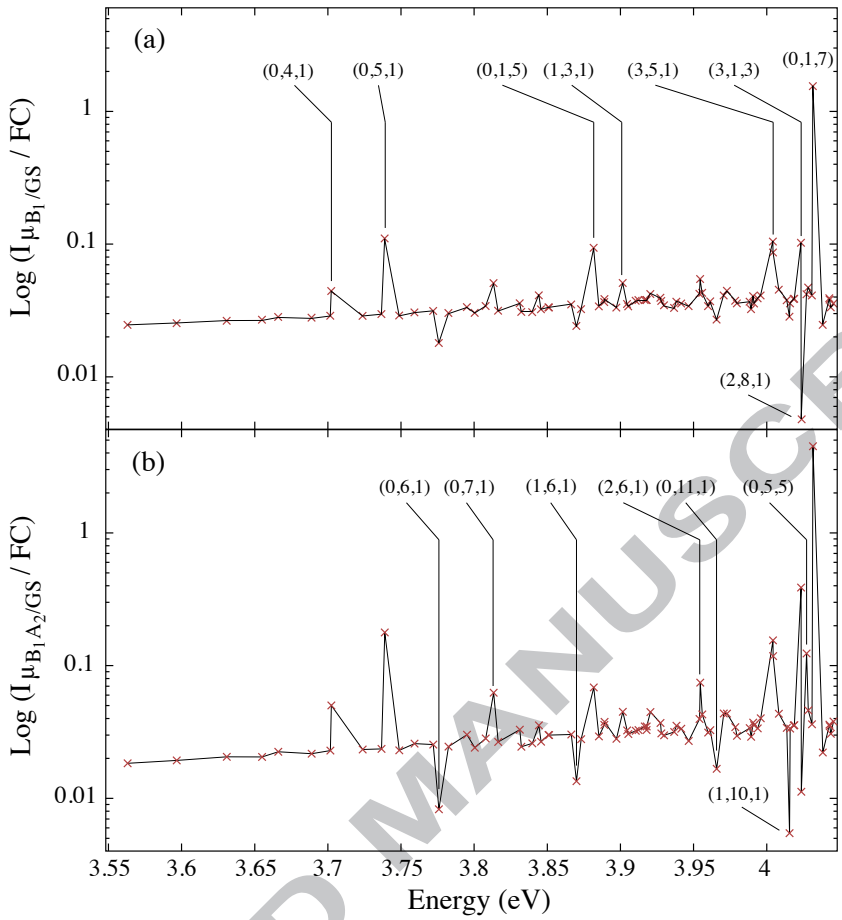

FIG. 7: (a) Ratio between the intensities obtained with and without considering the transition dipole between the GS and the 1^1B_1 state. (b) Same as (a) but including in addition the transition dipole for the 1^1A_2 state. The ratios are reported using a logarithmic scale, and the red crosses indicate the energies of the states, the black line is just added to guide the eyes. In both cases the non-Condon effects appear as a global shift of the intensities, but few transitions are strongly affected (indicated in the plot). Nonetheless, these transitions with or without the transition dipole remain weak and do not much affect the spectrum.

IV. CONCLUSIONS

In this work we have proposed an assignment of the low-energy part of the SO_2 absorption spectrum resulting from the coupled 1^1A_2 and 1^1B_1 states. We showed that the Clements bands A to D have only one common series consisting of (4,n_2,1) levels superposed on other transitions. We noticed that the regular increase of intensity of these bands is accidental, and the density of bright states is rather large in this region. We obtain the first absorption band (0,0,1) at 3.56 eV, which is slightly different from the experimental value. We re-emphasize that for higher energies (especially above 3.9 eV) the assignments are only approximate and also other vibrational wavefunctions contribute to the vibronic eigenstates. In addition, the non-Condon effects have been investigated and are found to be weak in the energy range considered here, with a global shift of the

intensity rather than a variation of the relative intensity of the transitions. General features of the time-dependent wavepacket identified earlier [14, 15] have been re-discovered in the quasi-resonant states associated with the Clements bands and also in some of the underlying eigenstates. Because of the low intensity of the first transition, it should be worthwhile to investigate the role of the hot bands that may occur, as well as more details of the triplet absorption bands.

V. ACKNOWLEDGMENTS

C. L. would like to thank Daniel Peláez for fruitful discussions and careful reading of the manuscript. C. L. gratefully thanks for the financial support of the Max-Planck-Institute für Kernphysik Heidelberg through the IMPRS Quantum Dynamics in Physics, Chemistry and Biology. Support from the ANR-09-BLAN-0031-01ATTO-WAVE is warmly acknowledged by C. L. and R. T. In addition, C. L. acknowledges support by the ERC-StG (Project No. 277767-TDMET) and the VKR center of excellence, QUSCOPE.

[1] W. W. Watson and A. E. Parker, Phys. Rev. **37**, 1484 (1931).
[2] J. H. Clements, Phys. Rev. **47**, 224 (1935).
[3] J. H. Asundi and R. Samuel, Proc. Ind. Acad. Sci. A **2**, 30 (1935).
[4] N. Metropolis, Phys. Rev. **60**, 295 (1941).
[5] A. E. Douglas, Can. J. Phys. **36**, 147 (1958).
[6] A. J. Merer, Discuss. Faraday Soc. **35**, 127 (1963).
[7] I. H. Hillier and V. R. Saunders, Mol. Phys. **22**, 193 (1971).
[8] J. C. D. Brand and R. Nanes, J. Mol. Spectr. **46**, 194 (1973).
[9] Y. Hamada and A. J. Merer, Can. J. Phys. **52**, 1443 (1974).
[10] Y. Hamada and A. J. Merer, Can. J. Phys. **53**, 2555 (1975).
[11] K. Kamiya and H. Matsui, Bull. Chem. Soc. Jpn. **64**, 2792 (1991).
[12] H. Katagiri, T. Sako, A. Hishikawa, T. Yazaki, K. Onda, K. Yamanouchi, and K. Yoshino, J. Mol. Struct. **413**, 589 (1997).
[13] A. Li, B. Suo, Z. Wen, and Y. Wang, Science in China Series B **49**, 4 (2006).
[14] H. Müller and H. Köppel, Chem. Phys. **183**, 107 (1994).
[15] C. Lévêque, A. Komainda, R. Taïeb, and H. Köppel, J. Chem. Phys. **138**, 044320 (2013).
[16] F. Gaillard, B. Scaillet, and N. T. Arndt, Nature **478**, 229 (2011).
[17] I. Halevy, M. T. Zuber, and D. P. Schrag, Science **318**, 1903 (2007).

[18] A. E. Bourassa, A. Robock, W. J. Randel, T. Deshler, L. A. Rieger, N. D. Lloyd, E. J. Llewellyn, and D. A. Degenstein, Science **337**, 78 (2012).

[19] C. Xie, X. Hu, L. Zhou, D. Xie, and H. Guo, J. Chem. Phys. **139**, 014305 (2013).

[20] C. Lévêque, R. Taïeb, and H. Köppel, J. Chem. Phys. **140**, 091101 (2014).

[21] C. Lévêque, D. Peláez, H. Köppel, and R. Taïeb, Nature Communications **5**, 3190 (2014).

[22] S. Mai, P. Marquetand, and L. González, J. Chem. Phys. **140**, 204302 (2014).

[23] C. Lévêque, H. Köppel, and R. Taïeb, J. Chem. Phys. **140**, 204303 (2014).

[24] I. Wilkinson, A. E. Boguslavskiy, J. Mikosch, J. B. Bertrand, H.-J. Wörner, D. M. Villeneuve, M. Spanner, S. Patchkovskii, and A. Stolow, J. Chem. Phys. **140**, 204301 (2014).

[25] MOLPRO is a package of ab initio programs written by H.-J. Werner, P. J. Knowles, G. Knizia, F. R. Manby, M. Schütz, P. Celani, T. Korona, R. Lindh, A. Mitrushenkov, G. Rauhut, K. R. Shamasundar, T. B. Adler, R. D. Amos, A. Bernhardsson, A. Berning, D. L. Cooper, M. J. O. Deegan, A. J. Dobbyn, F. Eckert, E. Goll, C. Hampel, A. Hesselmann, G. Hetzer, T. Hrenar, G. Jansen, C. Köppl, Y. Liu, A. W. Lloyd, R. A. Mata, A. J. May, S. J. McNicholas, W. Meyer, M. E. Mura, A. Nicklaß, D. P. O'Neill, P. Palmieri, D. Peng, K. Pflüger, R. Pitzer, M. Reiher, T. Shiozaki, H. Stoll, A. J. Stone, R. Tarroni, T. Thorsteinsson, M. Wang.

[26] S. R. Langhoff and E. R. Davidson, Int. J. Quantum Chem. **8**, 61 (1974).

[27] T. H. Dunning, J. Chem. Phys. **90**, 1007 (1989).

[28] H. Köppel, in Conical Intersections: Electronic Structure, Dynamics & Spectroscopy, edited by W. Domcke, D. Yarkony and H. Köppel p. 175 (2004).

[29] H. Köppel, W. Domcke, and L. S. Cederbaum, Adv. Chem. Phys. **57**, 59 (1984).

[30] A. Thiel and H. Köppel, J. Chem. Phys. **110**, 9371 (1999).

[31] S. Mahapatra and H. Köppel, J. Chem. Phys. **109**, 1721 (1998).

[32] H. Köppel, J. Gronki, and S. Mahapatra, J. Chem. Phys. **115**, 2377 (2001).

[33] H. Köppel and B. Schubert, Mol. Phys. **104**, 1069 (2006).

[34] S. Mahapatra, H. Köppel, L. S. Cederbaum, P. Stampfuß, and W. Wenzel, Chem. Phys. **259**, 211 (2000).

[35] E. V. Gromov, C. Lévêque, F. Gatti, I. Burghardt, and H. Köppel, J. Chem. Phys. **135**, 164305 (2011).

[36] D. Asturiol, B. Lasorne, G. A. Worth, M. A. Robb, and L. Blancafort, Phys. Chem. Chem. Phys. **12**, 4949 (2010).

[37] H. Köppel, B. Schubert, and H. Lischka, Chem. Phys. **343**, 319 (2008).

[38] L. Zheng, M. E. Madjet, and O. Vendrell, J. Chem. Phys. **138**, 094313 (2013).

[39] J. Farqhar, H. Bao, F. Gatti, and H.Thiemens, Science **289**, 756 (2000).

[40] S. Hattori, J. A. Schmidt, M. S. Johnson, S. O. Danielache, A. Yamada, Y. Ueno, and N. Yoshida, Proc. Natl. Acad. Sci. USA **110**, 17656 (2013).

[41] A. R. Whitehill, C. Xie, X. Hu, D. Xie, H. Guo, and S. Ono, Proc. Natl. Acad. Sci. USA **110**, 17697 (2013).

[42] P. Kumar, J. Ellis, and B. Poirier, Chem. Phys. **450-451**, 59 (2015).

[43] C. Lanczos, J. Res. Natl. Bur. Stand. **45**, 255 (1950).

[44] M. Beck, G. Worth, A. Jäckle, and H.-D. Meyer, Phys. Rep. **324**, 1 (2000).

[45] G. A. Worth and M. H. Beck and A. Jäckle and H.-D. Meyer. The MCTDH package, version 8.2, University of Heidelberg, Heidelberg, Germany, 2000; H.-D. Meyer, The MCTDH package, version 8.3, 2002 and version 8.4, 2007, see http://mctdh.uni-hd.de.

[46] F. Kuhnert, J. Appl. Math. Mech. **61**, 345 (1981).

[47] J. K. Cullum and R. A. Willoughby, Lanczos Algorithms for Large Symmetric Eigenvalue Problems, Birkhäuser, Basel (1985).

[48] R. Chen and H. Guo, J. Comput. Phys. **136**, 494 (1997).

[49] C. Iung and C. Leforestier, J. Chem. Phys. **90**, 3198 (1989).

[50] M. D. Feit, J. A. F. Jr., and A. Steiger, J. Comput. Phys. **47**, 412 (1982).

[51] R. T. Skodje, R. Sadeghi, and H. Köppel, J. Chem. Phys. **101**, 1725 (1994).

[52] R. Sadeghi and R. T. Skodje, J. Chem. Phys. **120**, 1746 (2004).

[53] S. Mahapatra, R. Vetter, C. Zuhrt, H. T. Nguyen, T. Ritschel, and L. Zülicke, J. Chem. Phys. **107**, 2930 (1997).

[54] R. Padmanaban and S. Mahapatra, J. Chem. Phys. **120**, 1746 (2004).

[55] K. Bogumil, J. Orphal, T. Homann, S. Voigt, P. Spietz, O. C. Fleischmann, A. Vogel, M. Hartmann, H. Kromminga, H. Bovensmann, et al., J. Photochem. Photobiol. A **157**, 167 (2003).

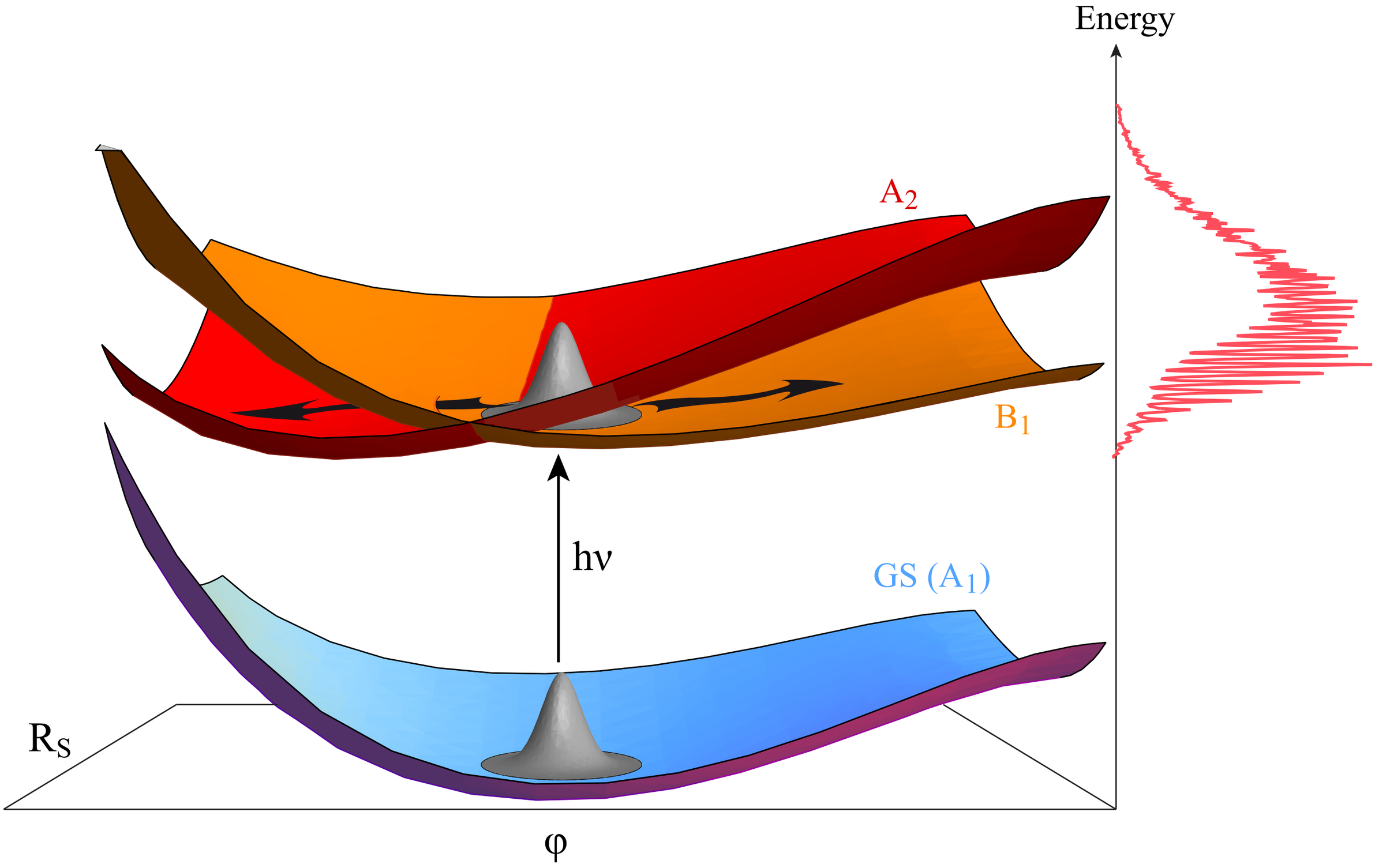
Energy
A2
B1
hν
GS (A1)
RS
φ

- theoretical assignment of the low-energy part of the absorption spectrum of SO_2
- Lanczos diagonalisation of the molecular vibrational Hamiltonian
- Comparison with the quasi-resonant states from time-dependent calculations
- Study of the non-Condon effects through the coordinate dependence of the transition dipole